Elastic properties and anisotropic pinning of the flux-line lattice in single-crystalline $La_{1.85}Sr_{0.15}CuO_4$

Tetsuo Hanaguri* and Tetsuo Fukase
Institute for Materials Research, Tohoku University, Sendai 980, Japan

Isao Tanaka and Hironao Kojima
Institute of Inorganic Synthesis, Yamanashi University, Kofu 400, Japan

(Received 14 October 1992; revised manuscript received 10 May 1993)

The temperature dependence of the sound velocity and the sound-attenuation coefficient in single-crystalline $La_{1.85}Sr_{0.15}CuO_4$ have been measured in the mixed state with an ultrasonic technique. An increase in the sound velocity and an attenuation peak, due to the elasticity of the flux-line lattice and the flux-pinning effect, are observed at a temperature lower than the superconducting transition temperature T_c. The compression and tilt moduli of the flux-line lattice are found to be softened in the case of $\mathbf{H}\perp\mathbf{c}$. The anisotropic activation energies that are necessary to depin the flux-line lattice are separately evaluated by measurements under various settings of the directions of the wave vector $\mathbf{k}$, the polarization vector $\mathbf{u}$, and the magnetic field $\mathbf{H}$ using an analysis based on the thermally assisted flux-flow model. The estimated activation energies are 1140 K (at 0 K, 6 T) for $\mathbf{H}\perp\mathbf{c}$, $\mathbf{u}\parallel\mathbf{c}$, 201 K (at 0 K, 14 T) for $\mathbf{H}\perp\mathbf{c}$, $\mathbf{u}\parallel(\mathbf{c}\times\mathbf{H})$, and 93 K (at 0 K, 6 T) for $\mathbf{H}\parallel\mathbf{c}$, $\mathbf{u}\perp\mathbf{c}$. These results are consistent with the intrinsic pinning mechanism. The activation energies determined by ultrasonic measurements are found to be smaller than those determined by resistivity measurements.

I. INTRODUCTION

Investigations of the physical properties of high-T_c oxide superconductors (HTSC's) in the mixed state are as interesting as attempts to find the mechanism of high T_c. Some characteristics of HTSC's, a short coherence length and a layer structure for example, make their mixed state distinctive. Because of the small coherence volume, the flux-pinning energy in HTSC's is relatively small and the pinned flux lines are easily depinned by small driving forces with the assistance of the thermal energy. Since the motion of flux lines yields an energy dissipation, it is important to find an effective flux-pinning mechanism in HTSC's. The first step to solve this problem is to determine the activation energy U which is necessary to depin the flux-line lattice (FLL). Some characteristic phenomena in HTSC's, such as the large relaxation of the magnetization[1] and the broadening of the resistive transition in magnetic fields,[2] are considered to be closely related to the thermally activated motion of flux lines. Therefore analyses of these phenomena are frequently used to estimate the activation energy U.

Regarding the layer structure of HTSC's, Campbell, Doria, and Kogan have pointed out that the structure of the FLL becomes anisotropic if an applied field is tilted form the c axis, which is perpendicular to conducting layers.[3] The flux-pinning effect is also influenced by the layer structure. In general, flux pinning is caused by imperfections in a superconductor such as defects, impurities, and grain boundaries. In addition to these, Tachiki and Takahashi have proposed an intrinsic pinning mechanism based on the layer structure.[4,5] They have pointed out that the layer structure brings the spatial variation of the order parameter along the c axis and the flux lines which lie in the c plane are naturally pinned at the position where the order parameter is the smallest. This mechanism is important only when flux lines move along the c axis. Therefore, in HTSC's, the flux-pinning effect should be anisotropic. To examine the anisotropy of the activation energy, it is important to understand the effective pinning mechanism of this system.

If the uniaxial anisotropy is assumed in HTSC's, there are three independent patterns of flux motion as illustrated in Fig. 1. For the magnetic field applied along the c axis, the direction of the flux motion is unique and is always perpendicular to the c axis [Fig. 1(a)]. For the magnetic field applied perpendicular to the c axis, two independent directions of flux motion are possible. One of

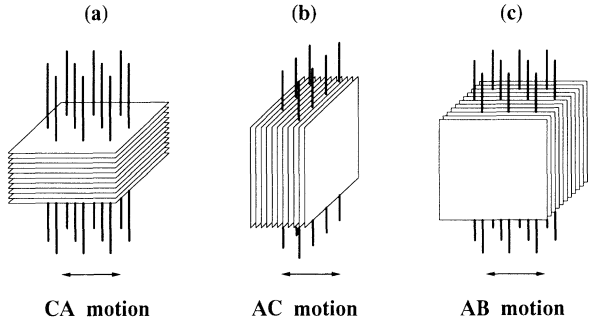

FIG. 1. Schematic illustrations of the three patterns of flux motions in HTSC's. The lines and planes indicate the flux lines and the stack of the CuO_2 planes, respectively. The arrows indicate the directions of the flux motions.

these is parallel to the c axis [Fig. 1(b)], and the other is perpendicular to both the applied field and the c axis [Fig. 1(c)]. Hereafter, the patterns of the motions in Figs. 1(a), 1(b), and 1(c) are referred as the CA motion, the AC motion, and the AB motion, respectively. The activation energies U's in different patterns of the motions should be different. The AC motion is related to the intrinsic pinning.

For the purpose of investigating the anisotropy of the FLL and activation energies, magnetization measurements cannot separate the AC motion from the AB motion. Although resistivity measurements can separate them using appropriate directions of currents and fields, it does not give us direct information about the nature of the FLL itself.

Pankert and co-workers have developed a novel method to study the FLL itself and the interaction between the FLL and crystal lattice (CL) using ultrasonic technique.[6–9] In a temperature region above the characteristic depinning temperature T_p, the pinning of the FLL vanishes effectively and one can regard the FLL as almost independent of the CL. Therefore, in this temperature region, the elastic constant measured by ultrasonic measurements only reflects the elastic constant of the CL. The depinning temperature T_p is governed by the frequency of ultrasound and the activation energy U. The latter depends on the magnetic field, temperature, and the pattern of the motion of flux lines. At temperatures below T_p, since the FLL is pinned to the CL, the sum of the elastic constants of the FLL and CL should be observed. Consequently, a step and a peak at T_p appear in the temperature dependence of the sound velocity and the sound-attenuation coefficient, respectively. The height of the step in the temperature dependence of the sound velocity reflects the elastic constant of the FLL, and the shapes of the step and the peak are governed by temperature and field dependence of the activation energy U.

Pankert[6,7] analyzed this process within the framework of the thermally assisted flux-flow (TAFF) model[10] and derived the temperature dependence of the sound velocity and the sound-attenuation coefficient in terms of the dc resistivity caused by the motion of flux lines.[6] Since sound waves are polarized, not only the anisotropy of the activation energies, but also various kinds of elastic constants can be obtained if experiments are performed on a single crystal. Furthermore, since ultrasonic measurement is a bulk-sensitive technique, contributions from minor but strong pinning centers (e.g., surface) to the activation energies can be neglected. In spite of these advantages, ultrasonic experiments for the purpose of investigating the relation between the FLL and CL have been performed only on polycrystalline samples.[8,9,11] In this paper we report ultrasonic investigations with respect to the elastic properties of the FLL and the anisotropic activation energies in single-crystalline $La_{1.85}Sr_{0.15}CuO_4$.

II. ELASTIC PROPERTIES OF THE FLL

First, we introduce the elastic moduli of the FLL. If the FLL forms a regular triangular lattice, there are three independent components in the elastic constant tensor of the FLL,[12] namely, c_{11}^f as the compression modulus, c_{44}^f as the tilt modulus, and c_{66}^f as the shear modulus. These moduli are expressed as[13,14]

$$c_{11}^f - c_{66}^f = \frac{B^2}{4\pi}\frac{dH}{dB} , \tag{1}$$

$$c_{44}^f = \frac{BH}{4\pi} , \tag{2}$$

$$c_{66}^f \simeq \frac{H_{c2}^2}{4\pi}\frac{(H/H_{c2})(1-H/H_{c2})}{8\kappa^2} . \tag{3}$$

Here B is the magnetic induction, H is the applied magnetic field, H_{c2} is the upper critical field, and κ is the Ginzburg-Landau parameter. The elastic constants $c_{11}^f - c_{66}^f$ and c_{44}^f are determined from thermodynamical arguments and are considered to be isotropic even in anisotropic superconductors. On the other hand, the shear modulus c_{66}^f is affected by the structure of the FLL and goes to zero if the FLL melts. Therefore c_{66}^f gives us information about the interaction between flux lines. Moreover, since the motion of a part of the FLL yields the shear deformation of the FLL, the activation energy U depends on the c_{66}^f.[15]

If an applied field exceeds the lower critical field and a magnetic penetration depth is long enough, one can assume that the magnetic induction B in the superconductor is almost uniform and nearly equal to the applied field H. In $La_{1.85}Sr_{0.15}CuO_4$ these conditions are sufficiently satisfied under magnetic fields above 1 T. In addition to this, c_{11}^f and c_{44}^f are at least 10^3 times larger than c_{66}^f in these fields. Therefore, in a good approximation, one can rewrite the elastic constants of the FLL as

$$c_{66}^f \ll c_{11}^f \simeq c_{44}^f \simeq \frac{H^2}{4\pi} . \tag{4}$$

Next, we show a procedure how to obtain the anisotropy of the activation energies U's from ultrasonic measurements. The sound velocity V_s and the sound-attenuation coefficient α in the mixed state can be written as

$$\rho V_s(H,T)^2 = c_{ij}^c(H,T) + \Delta c^f(H,T) , \tag{5}$$

$$\alpha(H,T) = \alpha^c(H,T) + \Delta\alpha^f(H,T) , \tag{6}$$

where ρ is the mass density. Here c_{ij}^c and α^c are the elastic constant of the CL and the sound-attenuation coefficient of the CL, respectively. In general, both c_{ij}^c and α^c are magnetic-field dependent mainly due to the suppression of superconductivity. In Eqs. (5) and (6), Δc^f and $\Delta\alpha^f$ are the contributions from the FLL and include information about U. Pankert and co-workers adopted the TAFF model to get definite formulas of Δc^f and $\Delta\alpha^f$.[6,7,9] Within the framework of the TAFF model, the motion of the FLL against the CL is described by a diffusion-type equation with a relaxation constant Γ which is related to U.[10] Solving the equations of motion, one gets the following formulas for Δc^f and $\Delta\alpha^f$: for $\mathbf{u}\|\mathbf{H}$,

$$\Delta c^f = 0, \quad \Delta\alpha^f = 0 ; \tag{7}$$

for $\mathbf{u}\perp\mathbf{H}$,

$$\Delta c^f = c_{ii}^f \frac{\omega^2}{\omega^2+(c_{ii}^f \Gamma k^2)^2} , \tag{8}$$

$$\Delta\alpha^f = \frac{\omega^2}{2\rho V_s(H,T)^3} c_{ii}^f \frac{c_{ii}^f \Gamma k^2}{\omega^2+(c_{ii}^f \Gamma k^2)^2} . \tag{9}$$

Here ω is the angular frequency of the ultrasound. Equation (7) implies that the FLL does not couple to the sound waves of which $\mathbf{u}$ is parallel to $\mathbf{H}$. The TAFF model can be applied when the current J used for the measurement satisfies the relation $J \ll J_c k_B T/U$.[16] Here k_B is the Boltzmann constant and J_c is the critical current above which energy gain, which is induced by the Lorentz force, overcomes U and Bardeen-Stephen-type flux flow occurs. Since the current J induced by the sound waves is very small compared to the current used in the other methods, such as resistivity measurements,[9] the TAFF region in ultrasonic measurements should be wide. In the TAFF region, since a linear response is expected,[16] one can check the validity of the TAFF model to confirm that Δc^f is independent of applied sound power.

The relaxation coefficient Γ can be related to the Ohmic TAFF resistivity σ^{-1} caused by the flux motion by the relation[6]

$$\sigma^{-1} = \Gamma \frac{4\pi}{c^2} \frac{B}{H} c_{44}^f , \tag{10}$$

where c is the light velocity . The activation energy U is related to σ^{-1} by the Arrhenius-like formula

$$\sigma^{-1} = \rho_0 \exp\left[-\frac{U}{k_B T}\right] . \tag{11}$$

Here ρ_0 is the proportional coefficient. In general, both ρ_0 and U depend on both field and temperature. Moreover, U depends on the pinning energy of each pinning center, number of the pinning centers, and the elasticity of the FLL in a complicated way.[15] For a real analysis of the experimental data, therefore, the field and temperature dependences of ρ_0 and U should be suitably assumed. The model we have adopted will be described later. Equations (10) and (11) represent the relation between Γ and U.

Since the relaxation coefficient Γ should be different in each pattern of the flux motion displayed in Fig. 1, the anisotropy of U can be obtained from ultrasonic measurements using various directions of $\mathbf{u}$. We define U_{CA}, U_{AC}, and U_{AB} as the activation energies which correspond to the FLL motions of CA, AC, and AB, respectively.

The elastic constants c_{ij}^c and c_{ii}^f also take different values if the directions of $\mathbf{u}$, $\mathbf{k}$, and $\mathbf{H}$ are changed. The values of c_{ij}^c, c_{ii}^f, and U_{IJ} for various configurations in $La_{1.85}Sr_{0.15}CuO_4$ are listed in Table I. It is well known that $La_{1.85}Sr_{0.15}CuO_4$ undergoes a structural phase transition from high-temperature tetragonal to orthorhombic at a temperature T_d above T_c.[17] Below T_d, the crystalline axes a and b are rotated 45° around the c axis. Since the crystal takes a twin structure in the orthorhombic phase,[18] the symmetry of the crystal can be assumed to be a quasitetragonal one even below T_d. Therefore we adopt the crystalline coordinates of the high-temperature tetragonal phase to express the crystallographic directions with suffix t. The $[100]_t$ axis is parallel to the diagonal line of the basal plane of the CuO_6 octahedron, and the $[001]_t$ axis is perpendicular to the CuO_2 planes.

It is necessary to extract Δc^f and $\Delta\alpha^f$ from Eqs. (5) and (6) to obtain U. Since c^c and α^c depend on the magnetic field, it is necessary to compare the results of two different configurations, namely $\mathbf{u}\|\mathbf{H}$ and $\mathbf{u}\perp\mathbf{H}$. The difference between these two results can be regarded as the contribution from the FLL. In both configurations the sound modes of the CL and the crystallographic directions of $\mathbf{H}$ must be the same. Here it is assumed that the effects of $\mathbf{H}$ on c^c and α^c only depend on the crystallographic direction of $\mathbf{H}$, but do not depend on the relative angle between $\mathbf{H}$ and $\mathbf{u}$. Possible combinations of each pattern of the flux motion are listed in Table II. Some combinations are not appropriate to estimate U's. First, the c_{66}^c mode cannot be measured by ultrasonic experiments because of the strong scattering of sound waves at the twin boundary below T_d.[19] Second, although the shear modulus of the FLL, c_{66}^f, plays an important role in U,[15] it would be difficult to measure c_{66}^f because it is very small. Conventional sound-velocity measurement systems have a resolution of 10^{-6}–10^{-7}, while the ratio between c_{66}^f and the elastic constant of the CL may be smaller than this value. Accordingly, we have measured the sound modes of the CL, c_{44}^c for U_{CA}, c_{44}^c for U_{AC}, and c_{11}^c for U_{AB}. In these modes the corresponding elastic constants of the FLL are c_{44}^f, c_{44}^f and c_{11}^f, respectively.

TABLE I. Elastic contents of the crystal lattice and the flux-line lattice measured under various settings of $\mathbf{k}$, $\mathbf{u}$, and $\mathbf{H}$.

	$\mathbf{H}\|[001]_t$						$\mathbf{H}\|[100]_t$					
	$\mathbf{u}\|[100]_t$		$\mathbf{u}\|[010]_t$		$\mathbf{u}\|[001]_t$		$\mathbf{u}\|[100]_t$		$\mathbf{u}\|[010]_t$		$\mathbf{u}\|[001]_t$	
$\mathbf{k}$	CL	FLL[a]	CL	FLL[a]	CL	FLL	CL	FLL	CL	FLL[b]	CL	FLL[c]
$[100]_t$	c_{11}^c	c_{11}^f	c_{66}^c	c_{66}^f	c_{44}^c	none	c_{11}^c	none	c_{66}^c	c_{44}^f	c_{44}^c	c_{44}^f
$[010]_t$	c_{66}^c	c_{66}^f	c_{11}^c	c_{11}^f	c_{44}^c	none	c_{66}^c	none	c_{11}^c	c_{11}^f	c_{44}^c	c_{66}^f
$[001]_t$	c_{44}^c	c_{44}^f	c_{44}^c	c_{44}^f	c_{33}^c	none	c_{44}^c	none	c_{44}^c	c_{66}^f	c_{33}^c	c_{11}^f

[a] U_{CA}.
[b] U_{BA}.
[c] U_{AC}.

TABLE II. Possible combinations of **k** and **u** to extract the contributions from the FLL, Δc^f and $\Delta\alpha^f$, in Eqs. (5) and (6). The elastic constants of the CL and FLL are also shown.

	Type	H⊥u		H∥u			
	of	FLL+CL		CL only		Elastic const.	
B	motion	k	u	k	u	CL	FLL
$[001]_t$	*CA*	$[001]_t$	$[100]_t$	$[100]_t$	$[001]_t$	c_{44}^c	c_{44}^f
$[100]_t$	*AC*	$[100]_t$	$[001]_t$	$[001]_t$	$[100]_t$	c_{44}^c	c_{44}^f
		$[010]_t$	$[001]_t$	$[001]_t$	$[100]_t$	c_{44}^c	c_{66}^f
	AB	$[100]_t$	$[010]_t$	$[010]_t$	$[100]_t$	c_{66}^c	c_{44}^f
		$[010]_t$	$[010]_t$	$[100]_t$	$[100]_t$	c_{11}^c	c_{11}^f
		$[001]_t$	$[010]_t$	$[001]_t$	$[100]_t$	c_{44}^c	c_{66}^f

III. EXPERIMENTAL DETAILS

A large and high-quality $La_{1.85}Sr_{0.15}CuO_4$ single crystal was grown by the traveling-solvent floating-zone technique.[20] For ultrasonic measurements the grown crystal was cut into a parallelepiped of which two pairs of planes are perpendicular to the $[100]_t$ and $[001]_t$ axes. Each pair of planes is polished carefully to be parallel and flat. The dimensions of the sample are 4.501 mm along the $[100]_t$ and 4.146 mm along the $[001]_t$ axis.

Sound waves were generated by $LiNbO_3$ transducers glued on the polished planes by RTV (Shin-etsu silicone KE347W). A Z cut one was used for longitudinal waves and an X cut for transverse waves. The temperature dependences of the sound velocity V_s and the sound-attenuation coefficient α were simultaneously measured by the phase-comparison and pulse-echo methods, respectively. The absolute value of V_s was determined by the pulse-superposition method at 4.2 K in the absence of a magnetic field. The magnetic-field dependence of V_s in the normal state and the change of the sample length can be neglected. The measuring frequencies were 21.7 MHz for the longitudinal c_{11}^c mode and 23.3 and 23.7 MHz for the transverse c_{44}^c mode.

Magnetic fields were generated by a 6-T superconducting magnet with a cancellation coil or a 15-T superconducting magnet. Temperature was monitored by platinum and germanium thermometers mounted at the position of zero field of the 6-T magnet or a carbon glass thermometer of which the magnetoresistance error has been already corrected. All of the data were taken in the warming process after field cooling. The superconducting transition temperature T_c was determined to be 33.5±3 K by a previous measurement of V_s in the c_{33}^c mode in which V_s exhibits a clear jump at T_c.[21]

For comparison, we also measured the resistivity along the $[110]_t$ and $[001]_t$ axes by the standard dc four-probe method under magnetic fields both parallel and perpendicular to the $[001]_t$ axis. Resistivity measurements were performed on the crystals which were different from the crystal used for ultrasonic measurements.

IV. RESULTS

Figure 2 shows the temperature dependence of the sound velocity V_s in the c_{44}^c mode measured under two settings of **k**, **u**, and **H**. In both configurations sound waves can couple to the FLL since the magnetic fields are applied perpendicular to **u**. The flux lines move as CA type in the configuration of Fig. 2(a) and move as AC type in the configuration of Fig. 2(b). The elastic constants of the FLL are c_{44}^f in both configurations. In the absence of a magnetic field, V_s is a smooth function of temperature in the whole temperature range including T_c. Under magnetic fields, V_s is enhanced in the low-temperature region below T_c in an anisotropic way.

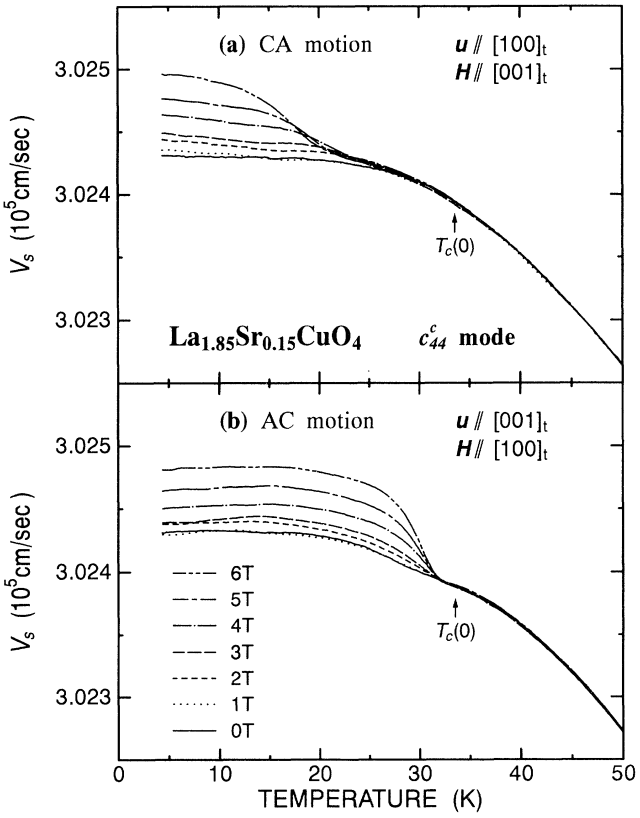

FIG. 2. Temperature dependence of the sound velocity V_s in the c_{44}^c mode measured under two settings of **k**, **u**, and **H**. In both configurations, the FLL couples to the sound waves.

Since there are no anomalies in V_s at T_c in the absence of a magnetic field, it seems that the strain e_{xz}, corresponding to the c_{44}^c mode, hardly couples to superconductivity. Therefore it is expected that there are few magnetic-field effects on c^c and α^c in the c_{44}^c mode. To confirm this the elastic constant c_{44}^c was measured under magnetic fields applied parallel to **u**. In the case of $\mathbf{k}\|[001]_t$ and $\mathbf{u}\|\mathbf{H}\|[100]_t$, we could not detect any magnetic-field dependence in V_s and α up to 6 T. On the other hand, in the case of $\mathbf{k}\|[100]_t$ and $\mathbf{u}\|\mathbf{H}\|[001]_t$, V_s slightly increases below 10 K under magnetic fields. Although the origin of this effect is not clear, we consider that the increase in V_s *above* 10 K measured under magnetic fields *perpendicular* to **u** in the c_{44}^c mode is the influence of the FLL elasticity.

In the case of the c_{11}^c mode, V_s exhibits a clear kink just below T_c and increases below T_c even in the absence of a magnetic field as shown in Fig. 3. Under magnetic fields applied perpendicular to **u**, V_s is enhanced at low temperatures and is reduced in the vicinity of T_c as shown in Fig. 3(a). This feature is considered to be the superposition of two effects, namely, the enhancement due to the elasticity of the FLL and the reduction due to the suppression of superconductivity. The pattern of flux motion in this configuration corresponds to the *AB* motion, and the elastic constant of the FLL is c_{11}^f.

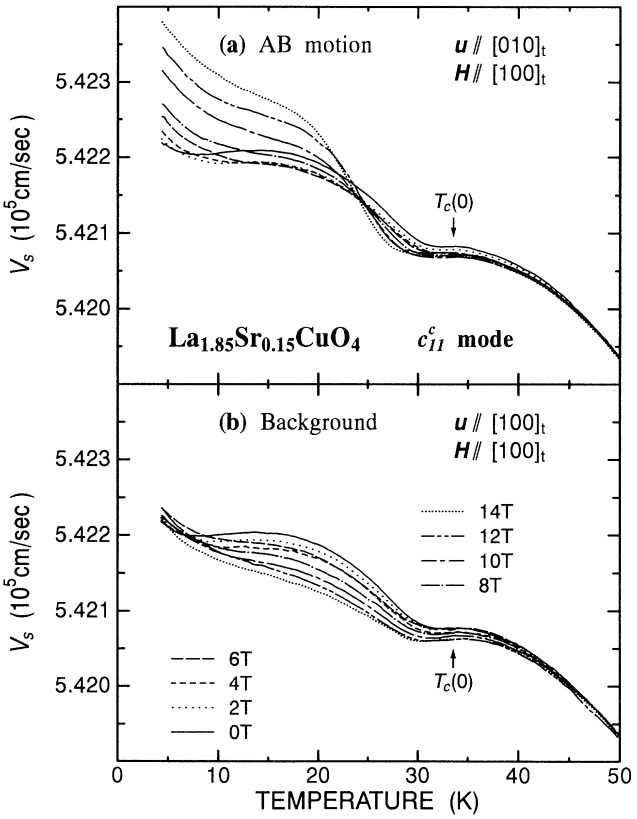

FIG. 3. Temperature dependence of the sound velocity V_s in the c_{11}^c mode under various magnetic fields. In the configuration of (a), the FLL couples to the sound waves. In the configuration of (b), the FLL does not couple to the sound waves.

To evaluate the influence of the suppression of superconductivity in the c_{11}^c mode, V_s and α were measured in a configuration in which magnetic fields were parallel to **u**. The results are shown in Fig. 3(b). In this configuration, V_s monotonically decreases with increasing magnetic field below T_c. Below about 10 K, magnetic fields have few effects on V_s.[21] Although the origins of these phenomena are indistinct, the results of this configuration can be used as a background to extract the elasticity of the FLL by comparing to the results of the configuration of Fig. 3(a).

The FLL contributions to V_s can be extracted for all patterns of flux motions shown in Fig. 1. In the case of the c_{44}^c mode, the data under magnetic fields are compared with the data in the absence of a magnetic field. In the case of the c_{11}^c mode, the data of Fig. 3(a) are compared to the data of Fig. 3(b). The temperature dependence of the excess elastic constants Δc^f's induced by the FLL are shown in Fig. 4. The value of the mass density 6.99 g/cm^3 was used to convert V_s to the elastic constant. Figures 4(a), 4(b), and 4(c) correspond to the flux motions of *CA*, *AC*, and *AB*, respectively. In each case, Δc^f exhibits a steplike anomaly at a temperature below T_c and comes to saturate in the low-temperature region as is expected from Eqs. (8), (10), and (11).

In order to confirm the validity of the TAFF model, the power dependence of Δc^f was measured in the case of the *CA* motion. Since it is difficult to measure the absolute value of the applied power to the transducer, we measured the relative power dependence of V_s. Even if the applied power is reduced to $\frac{1}{50}$, there are no changes in Δc^f except below 10 K where the background exhibits some magnetic-field dependence. Therefore, at temperatures above 10 K, the TAFF model can be safely used.

In addition to these experiments, we also measured V_s in the c_{44}^c mode in the configuration of $\mathbf{k}\|[001]_t$, $\mathbf{u}\|[100]_t$, and $\mathbf{H}\|[010]_t$ to detect the shear modulus of the FLL, c_{66}^f. However, we could detect no obvious changes in V_s up to 6 T ($\Delta V_s/V_s < \sim 10^{-5}$) in this configuration. Kogan and Campbell have pointed out that there are three different shear moduli of the FLL in an uniaxial superconductor.[22] The elastic constant c_{66}^f which we have measured corresponds to the smallest one among them and may be less than 10^{-6} of c_{44}^f. According to their theory, c_{66}^f, which is measured in the configuration of $\mathbf{k}\|[100]_t$, $\mathbf{u}\|[001]_t$, $\mathbf{H}\|[010]_t$, is strongly enhanced. It is interesting to measure this mode to examine the interaction between flux lines perpendicular to the *c* axis.

The shear modulus of the FLL, c_{66}^f, gives us direct information about the FLL melting. The FLL melting should be pronounced for $\mathbf{H}\|[001]_t$. However, it is difficult to measure c_{66}^f in this configuration. The reasons are as follows: First, the expected value of c_{66}^f is very small. [See Eq. (3).] Second, the c_{66}^c mode or the $(c_{11}^c - c_{12}^c)/2$ mode ($\mathbf{k}\|[110]_t$, $\mathbf{u}\|[1\bar{1}0]_t$) have to be measured to detect c_{66}^f in the case of $\mathbf{H}\|[001]_t$. However, the elastic constant of the CL, c_{66}^c, cannot be measured as we

mentioned before. Moreover, since the $(c_{11}^c - c_{12}^c)/2$ mode is strongly affected by the superconductivity,[19] it is difficult to extract the contribution from c_{66}^f.

V. DISCUSSION

First, we mention the magnetic-field dependence of Δc^f. At a sufficiently low temperature, the value of Δc^f is considered to be c^f itself because the FLL is nearly completely pinned to the CL. In Fig. 5 the values of Δc^f at 10 K are plotted against magnetic fields with double-logarithmic scales. The solid line indicates the theoretical curve expected from Eq. (4). When magnetic fields are applied parallel to the c axis (open circles), Eq. (4) holds well not only for the power of H, but also for the absolute value. On the other hand, if the magnetic fields are applied perpendicular to the c axis (solid squares and solid triangles), Eq. (4) holds for the power of H; however, the absolute value is reduced to about 75% of that expected from Eq. (4).

As the extrinsic origin of this reduction, the difference between B and H and/or an error in the absolute value of V_s are considered. However, the difference between B and H is estimated to be negligibly small ($\lesssim 10^{-3}$) from dc magnetization measurements. Furthermore, the error in the absolute value of V_s is estimated to be within a few percent in our experiments. Therefore the origin of this reduction, namely, the softening of the FLL, should be intrinsic.

It is pointed out that the elastic constants of the FLL are softened if the effective-mass anisotropy is taken into account.[23] This effect is remarkable in the AB motion. However, this effect can be observed only when the wavelength of the ultrasound reaches a value comparable to the London penetration depth λ_L; namely, the nonlocal effect becomes important.[24,25] In $La_{1.85}Sr_{0.15}CuO_4$, λ_L is estimated to be on the order of 10^{-5} cm.[26] In our experiments the wavelength is on the order of 10^{-2} cm. Since this value is much longer than λ_L, the nonlocal effect is negligible and the origin of the softening cannot be attributed to the mass anistropy only.

As the other explanation of the softening, flux motion in a pinning center can be considered. This effect be-

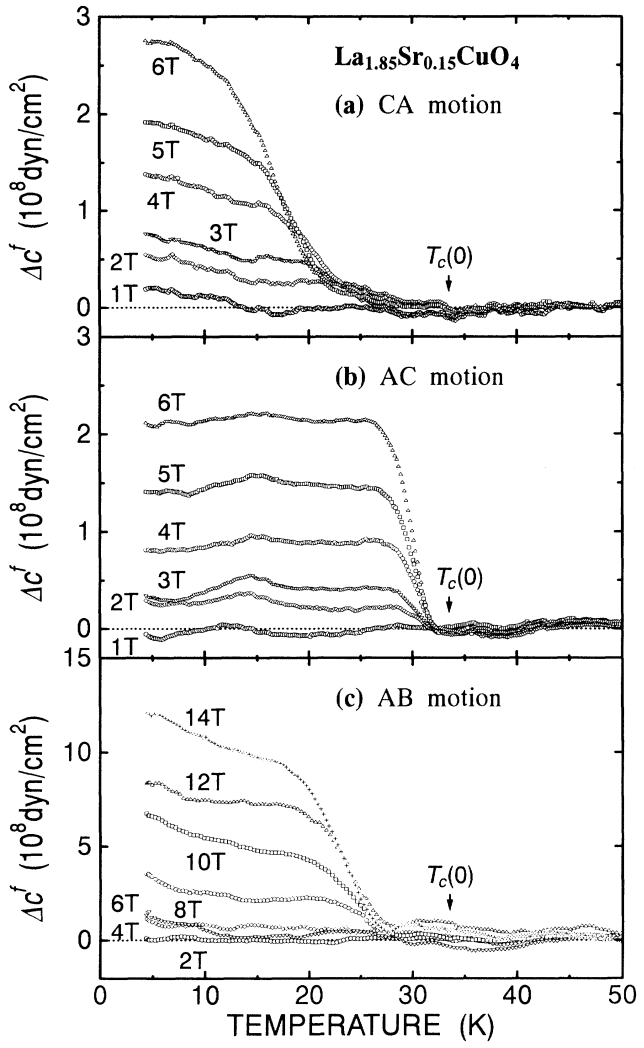

FIG. 4. Temperature dependence of the excess elastic constant Δc^f induced by the FLL for three patterns of the flux motions illustrated in Fig. 1.

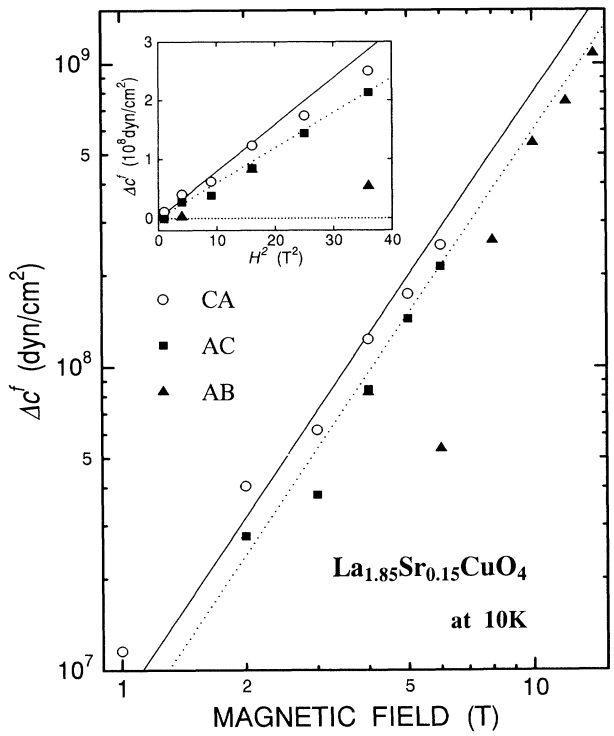

FIG. 5. Log-log plot of the magnetic field dependence of Δc^f at 10 K. The open circles indicate the data in the case of the CA motion ($\mathbf{H}\|\mathbf{c}$). The solid squares and solid triangles indicate the data in the cases of the AC motion and AB motion, respectively ($\mathbf{H}\perp\mathbf{c}$). The solid line is the theoretical curve expected from Eq. (4). The dotted line indicates 75% of the theoretical value. Inset: the plot against H^2 in a low-field region.

comes important when the current induced by the ultrasound reaches a value comparable to the critical-current density J_c. In our experiment, since the amplitude of the ultrasound is smaller than a few nm, the current induced by the ultrasound is estimated to be smaller than 10A/cm^2. Since J_c exceeds 10^3 A/cm^2 at 4.2 K up to 10 T,[27] the flux motion in a pinning center should be very small.

Although the origin of the softening is not clear, we introduce a correction factor γ to describe the magnitude of softening in following discussions. The factor γ is defined as

$$\gamma=\frac{c^f_{\rm obs}}{H^2/4\pi}\ , \tag{12}$$

where $c^f_{\rm obs}$ is the observed c^f_{ii} ($i=1$ or 4). In our case, $\gamma=1$ for $\mathbf{H}\|\mathbf{c}$ and $\gamma=0.75$ for $\mathbf{H}\perp\mathbf{c}$. The value of c^f_{ii} in Eqs. (8) and (9) should be replaced by γc^f_{ii}.

Next, we discuss the temperature dependence of Δc^f. Each pinning energy can be obtained by fitting the data of Fig. 4 to Eq. (8) with Eqs. (10) and (11). The temperature dependence of ρ_0 and U have to be assumed in Eq. (11). Here we adopt the model in which ρ_0 is temperature independent. The temperature dependence of U is assumed as follows:

$$U(T,H)=U(0,H)[1-T/T_c(H)]^n\ . \tag{13}$$

If the exponent n is 0, U is temperature independent and Eq. (11) is reduced to the simple Arrhenius formula. The magnetic-field dependence of ρ_0 and U can be evaluated by fitting the data taken under various magnetic fields to Eq. (8) with Eqs. (10), (11), and (13). To estimate the exponent n, we first analyze the resistivity data. Arrhenius plots of the resistivity data are shown in Fig. 6 for each pattern of the flux motion. As seen in the figure, all of the traces have negative curvature. This result implies that the exponent n takes positive finite value. Low-resistivity regions of the data are well expressed if n is assumed to be 1.5. Here ρ_0, U, and $T_c(H)$ are used as fitting parameters. Fitted curves using Eqs. (11) and (13) are also shown in Fig. 6 by solid lines. The parameters used in the fitting are listed in Table III. The activation energies deduced from resistivity measurements are indicated with a superscript r. The activation energies U^r_{ij}'s at 0 K decrease with increasing field. Suzuki has already analyzed the resistivity of a $La_{1.85}Sr_{0.15}CuO_4$ thin film

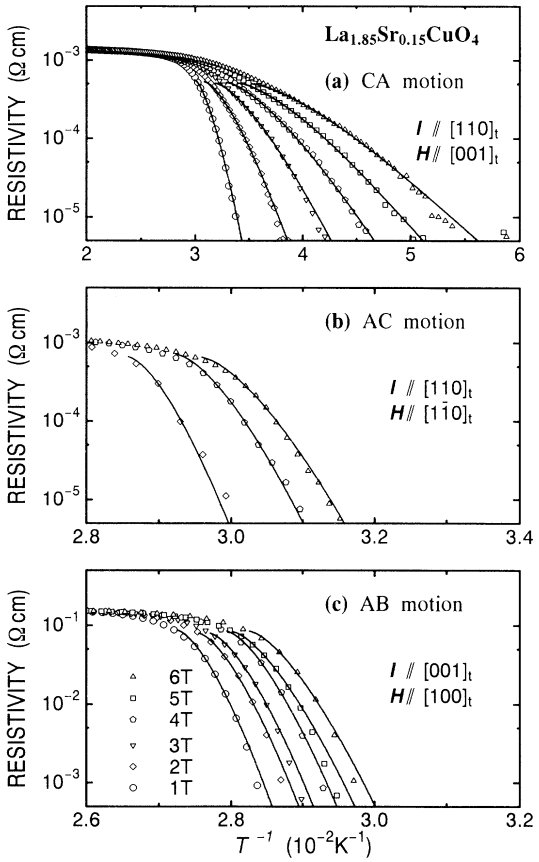

FIG. 6. Arrhenius plots of the resistivity data taken under various configurations. The solid lines indicate the fitted curves using Eqs. (11) and (13). The parameters used in fitting are listed in Table III.

and reported that values of n are 3 and 2.5 in the cases of $\mathbf{H}\|\mathbf{c}$ and $\mathbf{H}\perp\mathbf{c}$, respectively.[28] The discrepancy between his and our results may come from the different nature of the effective pinning mechanisms between a thin film and a bulk single crystal.

Using the exponent $n=1.5$ and varying U and ρ_0, the temperature dependences of Δc^f are fitted. Typical fitted curves with the experimental data are shown in Fig. 7. In the case of the AC motion, experimental results are well fitted by Eq. (8) as shown in Fig. 7(b). In other cases, al-

TABLE III. Fitted results of $T_c(H)$, ρ_0, and $U^r_{ij}(0,H)$ deduced from the resistivity data taken under various magnetic fields.

	CA motion			AC motion			AB motion		
H (T)	T_c (K)	ρ_0 (10^{-4} Ω cm)	U^r_{CA} (10^2 K)	T_c (K)	ρ_0 (10^{-4}Ω cm)	U^r_{AC} (10^4 K)	T_c (K)	ρ_0 (10^{-2} Ω cm)	U^r_{AB} (10^4 K)
1	33.4	5.6	30	35.2			36.7	8.8	1.81
2	32.4	5.3	13.5	35.0	6.7	1.63	36.3	8.0	1.65
3	31.4	5.1	8.52	34.6			36.1	8.0	1.57
4	30.4	5.2	6.22	34.2	7.2	1.18	35.8	8.5	1.45
5	29.4	5.1	4.66	34.0			35.7	8.4	1.24
6	28.4	5.0	3.59	33.8	6.6	0.97	35.4	8.5	1.20

though Eq. (8) holds well in the high-temperature region, experimental results deviate from the calculated curves in the low-temperature region as shown in Figs. 7(a) and 7(c). Since resistivity measurements do not have a sufficient resolution in the temperature region where the deviation occurs, it is not clear whether this deviation is only observed in ultrasonic measurements or not. The origin of the deviation might be due to the change of the effective pinning mechanism or the inhomogeneous deformation of the FLL due to the distribution of the pinning energies. In the latter case, the TAFF model should not be appropriate because nonlinear effects may set in. This is not contradictory to the power dependence of Δc^f below 10 K.

The parameters used in fitting are listed in Table IV. The activation energies U's deduced from ultrasonic measurement are indicated with a superscript u. The activation energies U_{ij}^u's decrease with increasing field, similarly to the case of the U_{ij}^r's. However, U_{ij}^u is smaller than U_{ij}^r in each pattern of flux motion. This result may imply that the effective pinning mechanism in ultrasonic measurements is different from that in resistivity measurements. Therefore, it is possible to assume different temperature dependences between U_{ij}^u and U_{ij}^r. For this reason we also tried to fit the data in Fig. 4 with $n=0$ (simple Arrhenius formula). To fit the data with $n=0$ was also possible as in the case of $n=1.5$. It was difficult to determine the temperature dependence of U from ultrasonic data only. The activation energies in the case of $n=0$ are 71 K at 6 T in the CA motion, 537 K at 6 T in the AC motion, and 132 K at 14 T in the AB motion. The order of magnitude and the anisotropy of the activation energies agree in both assumptions of n.

The difference between the results from resistivity measurements and the results from ultrasonic measurements are considered as follows: Since flux lines move over a macroscopic scale during resistivity measurements, they are affected by pinned flux lines and minor but strong pinning centers including surfaces and cracks which are not related to the bulk pinning. On the other hand, in the case of ultrasonic measurements, flux lines move only around their equilibrium positions. Therefore flux lines only "feel" the influence of pinning centers close to their equilibrium positions. Consequently, it is regarded that the real bulk pinning effect is reflected on U_{ij}^u.

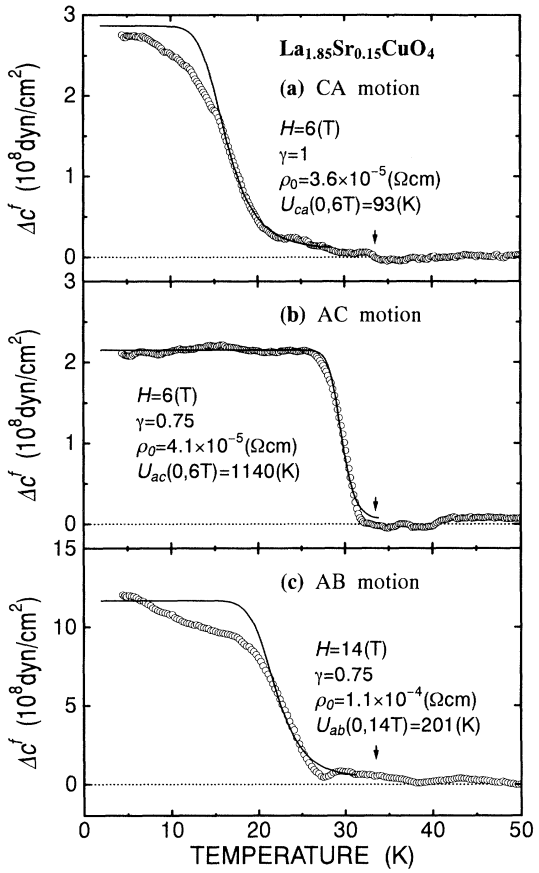

FIG. 7. Typical fitted results of the experimental data of Fig. 4 using Eqs. (8), (10), (11), and (13). The exponent n in Eq. (13) is assumed to be 1.5. The open circles indicate the experimental data, and the solid curves are the fitted curves. The arrows indicate $T_c(0)$. The parameters used in fitting are listed in Table IV.

Next, we discuss about the anisotropy of the pinning energies. In the case of resistivity measurements, U_{AC}^r is nearly equal to U_{AB}^r and U_{CA}^r is the smallest among the U^r's. This result implies that the intrinsic pinning mechanism is not dominant for resistivity measurements and

TABLE IV. Fitted results of $T_c(H)$, ρ_0, and $U_{ij}^u(0,H)$ deduced from the sound-velocity taken under various magnetic fields.

	CA motion			AC motion			AB motion		
H (T)	T_c (K)	ρ_0 (10^{-5} Ω cm)	U_{CA}^u (10^2 K)	T_c (K)	ρ_0 (10^{-5} Ω cm)	U_{AC}^u (10^3 K)	T_c (K)	ρ_0 (10^{-4} Ω cm)	U_{AB}^u (10^2 K)
2	32.4	~3.5	~4.2	35.0	10.9	1.50			
3	31.4	~2.7	~1.5	34.6	4.1	0.77			
4	30.4	3.3	1.47	34.2	4.6	1.22			
5	29.4	4.6	1.40	34.0	3.9	1.09			
6	28.4	3.6	0.93	33.8	4.1	1.14			
8							33.1	1.4	2.70
10							32.5	1.1	2.08
12							31.9	1.1	2.28
14							31.3	1.1	2.01

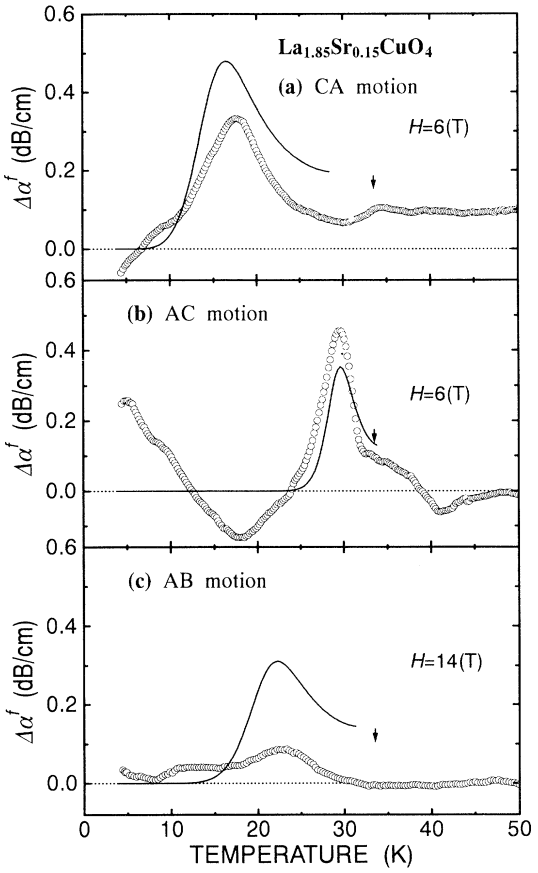

FIG. 8. Excess attenuation $\Delta\alpha^f$ induced by the FLL with calculated curves using Eq. (9) and the parameters listed in Table IV. The open circles indicate the experimental data, and the solid curves are the calculated ones. The arrows indicate $T_c(0)$.

U^r_{AC} and U^r_{AB} are governed by some other pinning centers. In the case of ultrasonic measurements, U^u_{AC} is the largest among the U^u's. Therefore it is suggested that the intrinsic pinning mechanism works well for the bulk-sensitive measurement. In other patterns of flux motion, U^u_{CA} is smaller than U^u_{AB}. In U^u_{CA} and U^u_{AB}, the pinning centers should not be the intrinsic one, but be some imperfections. The anisotropy between U^u_{CA} and U^u_{AB} is considered to be due to the anisotropy of H_{c2} and/or the anisotropy of the effective pinning center itself. In the case of the $YBa_2Cu_3O_7$ system, it is considered that twin planes act as the effective pinning center.[29] In $La_{1.85}Sr_{0.15}CuO_4$, since twin planes are parallel to the $(100)_t$ plane,[30] they can contribute to both U^u_{CA} and U^u_{AB}. For the purpose of making clear the role of twin planes, the measurement of the $(c^c_{11}-c^c_{12})/2$ mode will be meaningful. Comparing the two results in the cases of $\mathbf{H}\|[110]_t$ and $\mathbf{H}\|[1\bar{1}0]_t$, the FLL contribution can be extracted by the same process which was mentioned before. In this case, since the direction of FLL motion is not perpendicular to the twin planes, the value of U^u_{AB} which does not include the effect of twin planes can be estimated. This experiment is now in progress.

Brandt calculated the TAFF diffusivity Γ (Ref. 31) using the scaling prescription proposed in Ref. 23. According to his result, the order of the activation energies, namely, the order of Γ, is expected to be $U_{AC} > U_{CA} > U_{AB}$ if the effective-mass anisotropy only is taken into account. Since this result is inconsistent with our experimental result, the effective pinning center in $La_{1.85}Sr_{0.15}CuO_4$ may have an anisotropic character to its nature.

The temperature dependence of $\Delta\alpha^f$ is calculated using Eq. (9) and the parameters listed in Table IV. The results are shown in Fig. 8 with experimental data. The increase in $\Delta\alpha^f$ below about 15 K in the AC motion comes from the subtraction process of the background. Although it is not clear whether this effect is intrinsic or not, we have a feeling that this is an extrinsic effect, because the magnetic-field dependence of the attenuation is not systematic in this temperature region, while the peak at T_p systematically changes with changing magnetic field. Near T_p, the agreement between experimental results and calculated curves is good except for absolute values. More precise attenuation measurement is necessary to discuss the shape of the peaks.

In summary, the FLL elasticity and its anisotropic pinning have been investigated in a single-crystalline $La_{1.85}Sr_{0.15}CuO_4$ by the ultrasonic technique. This method is a bulk-sensitive measurement and is useful to investigate the anisotropy of the FLL if the measured elastic mode is suitably selected. The softening of the FLL is observed when magnetic fields are applied perpendicular to the c axis. The temperature dependence of the excess elastic constant and the sound-attenuation coefficient induced by the FLL are explained by the model based on the thermally assisted flux-flow model. Three independent pinning energies U^u_{CA}, U^u_{AC}, and U^u_{AB} have been evaluated separately, and it is found that $U^u_{AC} > U^u_{AB} > U^u_{CA}$. This result is consistent with the intrinsic pinning mechanism. The activation energies deduced from resistivity measurements are larger than those deduced from ultrasonic measurements. Therefore it is suggested that the effective pinning centers are different between these two measurements.

ACKNOWLEDGMENTS

The authors would like to thank to Professor T. Matsushita (Kyushu Institute of Technology) and Professor N. Kobayashi (I.M.R.) for variable discussions and comments. This work is supported by the Grant-in-Aid for Scientific Research on Priority Areas, "Mechanism of Superconductivity" and "Science of High T_c Superconductivity," from the Ministry of Education, Science and Culture of Japan.

*Present address: Department of Pure and Applied Sciences, University of Tokyo, Komaba, Tokyo 153, Japan.

[1]Y. Yeshurun and A. P. Malozemoff, Phys. Rev. Lett. **60**, 2202 (1988).
[2]T. T. M. Palstra, B. Batlogg, L. F. Schneemeyer, and J. V. Waszczak, Phys. Rev. Lett. **61**, 1662 (1988).
[3]L. J. Campbell, M. M. Doria, and V. G. Kogan, Phys. Rev. B **38**, 2439 (1988).
[4]M. Tachiki and S. Takahashi, Solid State Commun. **70**, 291 (1989).
[5]M. Tachiki and S. Takashashi, Solid State Commun. **72**, 1083 (1989).
[6]J. Pankert, Physica C **168**, 335 (1990).
[7]J. Pankert, Physica B **165&166**, 1272 (1990).
[8]J. Pankert, G. Marbach, A. Comberg, P. Lemmens, P. Frönig, and S. Ewert, Phys. Rev. Lett. **65**, 3052 (1990).
[9]P. Lemmens, P. Frönig, S. Ewert, J. Pankert, G. Marbach, and A. Comberg, Physica C **174**, 289 (1991).
[10]P. H. Kes, J. Aarts, J. van den Berg, C. J. van der Beek, and J. A. Mydosh, Supercond. Sci. Technol. **1**, 242 (1989).
[11]Y. Horie, T. Miyazaki, and T. Fukami, Physica C **175**, 93 (1991).
[12]A. M. Campbell and J. E. Evetts, Adv. Phys. **21**, 199 (1972).
[13]R. Labusch, Phys. Status Solidi **32**, 439 (1969).
[14]E. H. Brandt, J. Low Temp. Phys. **26**, 735 (1977).
[15]A. I. Larkin and Yu. N. Ovchinnikov, J. Low Temp. Phys. **34**, 409 (1979).
[16]E. H. Brandt, Physica C **195**, 1 (1992).
[17]M. François, K. Yvon, P. Fisher, and M. Decroux, Solid State Commun. **63**, 35 (1987).
[18]Y. Watanabe, T. Hanaguri, T. Fukase, I. Tanaka, and H. Kojima, Jpn. J. Appl. Phys. **27**, 2218 (1988).
[19]T. Suzuki, T. Fujita, M. Nohara, Y. Maeno, I. Tanaka, and H. Kojima, *Mechanisms of Superconductivity,* JJAP Series Vol. 7 (Publication office, Japanese Journal of Applied Physics, Tokyo, 1992), p. 219.
[20]I. Tanaka, K. Yamane, and H. Kojima, J. Cryst. Growth **96**, 711 (1989).
[21]T. Hanaguri, R. Toda, T. Fukase, I. Tanaka, and H. Kojima, Physica C **185-189**, 1395 (1991).
[22]V. G. Kogan and L. J. Campbell, Phys. Rev. Lett. **62**, 1552 (1989).
[23]G. Blatter, V. B. Greshkenbein, and A. I. Larkin, Phys. Rev. Lett. **68**, 875 (1992).
[24]A. Sudbø and E. H. Brandt, Phys. Rev. Lett. **66**, 1781 (1991).
[25]A. Sudbø and E. H. Brandt, Phys. Rev. B **43**, 10 428 (1991).
[26]G. Aeppli, R. J. Cava, E. J. Ansaldo, J. H. Brewer, S. R. Kreitzman, G. M. Luke, D. R. Noakes, and R. F. Kiefl, Phys. Rev. B **35**, 7129 (1987).
[27]K. Kishio, Y. Nakayama, T. Kobayashi, T. Noda, T. Kimura, K. Kitazawa, and K. Yamafuji, Physica C **185-189**, 2523 (1991).
[28]M. Suzuki, Physica C **185-189**, 2343 (1991).
[29]W. K. Kwok, U. Welp, G. W. Crabtree, K. G. Vandervoort, R. Hulscher, and J. Z. Liu, Phys. Rev. Lett. **64**, 966 (1990).
[30]T. Onozuka, M. Omori, M. Hirabayashi, and Y. Syono, Jpn. J. Appl. Phys. **26**, 1714 (1987).
[31]E. H. Brandt, Phys. Rev. Lett. **68**, 3769 (1992).